Histol Histopathol (2023) 38: 1465-1474

Histology and Histopathology
From Cell Biology to Tissue Engineering

ORIGINAL ARTICLE Open Access

Clinicopathological features and genomic analysis of bronchiolar adenoma

Jiaqi Bo[1]*, Xue Chen[1]*, Tingting Zhang[1]*, Xuyou Zhu[1]*, Long Zhang[1], Yuting Liu[1], Haoyang Zhang[1], Caixia Wu[1], Shunyan Mou[1], Xianghua Yi[1], Weiwei Rui[2] and Yu Zeng[1]

[1]Department of Pathology, Tongji Hospital, Tongji University School of Medicine and [2]Department of Pathology, Ruijin Hospital, Shanghai Jiao Tong University School of Medicine, Shanghai, China

*Co-first author

Summary. Background. Bronchiolar adenoma (BA) is a rare tumor of the bronchioles with a double-layer structure, including the basal cell layer and the superficial cell layer, and it has a good prognosis. However, the concept of a putative variant of BA has been proposed in the recent literature.

Methods. Data on 17 cases of BA were collected from our center. The clinical data, morphology, immunophenotype, and molecular changes were retrospectively analyzed. We also collected the molecular changes in BA reported in the previous literature and summarized the putative driver mutations of BA.

Results. Out of 17 BAs, 13 were classic cases with a double-layer structure, including 9 proximal-type and 4 distal-type BAs. Of note, we also identified 3 cases that lacked a continuous basal cell layer, including 2 cases of mixed-type BA with monolayered lesions (basal cells were undetected in some areas) and 1 case of a monolayered BA-like lesion (basal cells were completely undetected). The immunohistochemical findings of monolayer cell lesions were closer to those of minimally invasive adenocarcinoma. We also found one case in which BA transformed into invasive adenocarcinoma accompanied by mutations in the *TP53*, *JAK2*, *NF1* and *RB1* genes. Combined with the previous literature, the most common putative driver gene mutations in 62 BA lesions were *EGFR* (25/62; 41.0%) and *BRAF* (21/62; 34.4%).

Conclusion. Typical BA has a double-layer cell structure; however, there is also a putative variant of BA, which has a monolayer cell structure and lacks the basal cell layer. Transformation from BA into invasive adenocarcinoma is unusual but can occur.

Key words: Bronchiolar adenoma, Monolayered lesions, *EGFR*, *BRAF*

Corresponding Author: Yu Zeng, Xianghua Yi, Department of Pathology, Tongji Hospital, Tongji University School of Medicine, 389, Xincun Road, Putuo District, Shangai 200065, China, e-mail: yuzeng2013@163.com; yixhxf@163.com and Weiwe Rui, Department of Pathology, Ruijin Hospital, Shangai Jiao Tong University School of Medicine, No. 197, Ruijin 2nd Road, Huangspu District, Shangai, China, e-mail: rww11847@rjh.com.cn

www.hh.um.es. DOI: 10.14670/HH-18-609

Introduction

Bronchiolar adenoma (BA) is a benign lung tumor derived from bronchiolar epithelial cells that are characterized by double-layer architecture and bronchiolar differentiation. Based on morphology and immunophenotype, BA is divided into proximal and distal types (Chang et al., 2018). In 2002, Ishikawa first reported a ciliated mucoid papillary tumor (CMPT) case, which opened the way for research on the morphological characteristics, immunophenotype, and molecular genetics of CMPT (Ishikawa, 2002). An increasing number of observations and analyses of this kind of tumor have revealed that a papillary structure is not a necessary diagnostic criterion, as many such tumors lack a papillary structure, mainly comprising flat or glandular-like structures. However, CMPTs commonly present with a double-layer cell structure composed of the basal cell layer and the cavity surface cell layer, having a morphology similar to the histological morphology of bronchioles. Subsequently, Chang et al. proposed the diagnostic term bronchiolar adenoma (Chang et al., 2018). Recently, bronchiolar adenoma/ciliary mucoid papillary tumor (BA/CMPT) was recognized as a new entity in the adenoma subgroup in the 2021 World Health Organization classification of lung tumors (Nicholson et al., 2021). A double-layer cell structure and ciliated cells on the cavity surface are the main morphological features of bronchiolar adenomas. Moreover, immunohistochemical staining of TTF-1, P63, P40, and CK5/6 can help diagnose and classify bronchiolar adenoma. At the same time, BA/CMPT has

a high frequency of driving gene changes, including BRAF, EGFR, KRAS, and similar genes (Kao and Yeh, 2021). BA is recognized as a neoplasm with a benign clinical course; however, there are individual reports suggesting that BA has malignant potential, including diffuse pulmonary nodules, aggressive growth, and transformation into invasive mucinous adenocarcinoma (Miyai et al., 2018; Sun et al., 2020; Chen et al., 2021).

Herein, we present 17 cases of bronchiolar adenoma and discuss the clinicopathological and molecular genetic characteristics of this tumor based on the previously published literature. We also found three cases that were putative variants of BA and performed a detailed analysis of their morphology, immunohistochemistry, and gene mutations by next-generation sequencing (NGS).

Materials and methods

Patients and Clinicopathological Analysis

A retrospective search of archives and consultation slices in the Department of Pathology, Tongji Hospital, School of Medicine, Tongji University generated a total of 17 cases of bronchiolar adenoma between 2019 and 2022. The clinical features were reviewed for all cases, and the histological features were analyzed on the resection specimens. According to the proportion of mucous cells and ciliated cells in luminal cells, BA lesions were classified into proximal and distal types. Luminal cells lacked mucinous and ciliated cells in the distal type. The proximal type was classified into papillary and flat according to different histological structures, while the distal type was mainly flat.

Immunohistochemistry

All lesions were immunohistochemically stained. Primary antibodies included P63 (clone UMAB4, 1:100; ZSGB-BIO), P40 (clone BC28, 1:100; ZSGB-BIO), CK5/6 (clone OTI1F8, 1:100; ZSGB-BIO), thyroid transcription factor-1 (TTF-1) (clone SPT24, 1:100; ZSGB-BIO), Napsin A (clone IP64, 1:100; Gene Tech), Ki67 (clone UMAB107, 1:100; ZSGB-BIO), HNF-4α (clone K9218, 1:200; Abcam), P53 (clone MX008, 1:150; MXB), NF (clone 2F11, ready-to-use, MXB), RB (clone 1F8, ready-to-use, MXB), JAK2 (clone D2E12, 1:400, Cell Signaling Technology), and p-STAT3 (Tyr705) (clone D3A7, 1:600, Cell Signaling Technology). IHC was performed following standard procedures of the Envision two-step method on Dako automated instruments (Dako Autostainer Link48). IHC stains that were submitted from outside institutions were also reviewed.

Molecular analysis

Molecular analysis was performed on 9 out of 17 cases. DNA extraction was performed by using standard methods on formalin-fixed paraffin-embedded tissue and was performed on tumor tissue for 9 cases. DNA was purified using a TIANamp FFPE DNA Kit (TIANGEN

Table1. Clinicopathologic Features of BAs.

Cases	Age/Sex	Site/Size (cm)	Smoking History	Radiology (CT)	Morphology	Architecture	TTF-1 in Luminal cell	TTF-1 in Basal cell	Napsin A in Luminal cell	P63 in Basal cell	CK5/6 in Basal cell	Ki67	Clinical follow-up (months)
1	57/F	RLL/0.5	No	Hybrid ground glass opacity	Proximal	Flat	Weak +	+	+	+	+	2%	9
2	48/F	RLL/2.2	No	Ground-Glass Nodule, Lobulated, Spiculation	Mix type	Papillary/Flat	Weak +/–	+/NA	Partial +	+/NA	+/NA	2%	7
3	28/M	LLL/2	Yes	Irregular nodular foci with a partially solid component; Vacuole sign	Proximal	Papillary/Flat	+	+	+	+	+	2%	7
4	67/M	RLL/0.5	Yes	Ground-Glass Opacity	Distal	Flat	+	+	–	+	+	3%	6
5	69/F	RUL/0.5	No	Solid nodule, Lobulated, Spiculation	Proximal	Flat	Weak +	+	–	+	+	2%	5
6	55/F	LLL/0.5	No	Solid nodule	Proximal	Flat	–	+	Partial +	+	+	2%	4
7	73/F	RLL/1	No	Non solid nodule	Proximal	Flat	+	+	Partial +	+	+	2%	21
8	57/F	LLL/1.1	No	Conglomerate shadow	Distal	Flat	+/Weak +	+	+	+	+	2%	9
9	51/F	RLL/2.5	NA	NA	Proximal	Papillary	Weak +/–	+	–	+	+	2%	11
10	53/F	RLL/5.3	Yes	Conglomerate shadow, Lobulated, Spiculation	Proximal	Flat	+	+	+	+	+	3%	6
11	47/F	LUL/0.2	No	Ground-Glass Nodule	Distal	Flat	+	+	+	+	+	1%	5
12	47/M	RLL/1.5	Yes	Ground-Glass Opacity	Proximal	Papillary/Flat	Weak +	+	Partial +	+	+	2%	7
13	66/M	RLL/0.5	Yes	Solid nodule	Proximal	Papillary/Flat	Weak +	+	Partial +	+	+	1%	6
14	58/M	LLL/0.6	Yes	Hybrid ground glass nodule	Distal	Flat	+	+	+	+	+	1%	4
15	70/F	RLL/0.6	No	Ground-Glass Opacity	Mix type	Flat	Weak +/–	+/NA	Partial +	+/NA	+/NA	1%	2
16	60/M	RLL/1.3	No	Ground-Glass Opacity	Monolayered type	/	+	NA	–	NA	NA	2%	0.5
17	65/M	LLL/2.1	Yes	Solid nodule	BA with invasive adenocarcinoma	/	+	+/-	+/-	+/-	+/-	1-5%	28

F, Female; M, Male; RLL, Right Lower Lung; LLL, Left Lower Lung; RUL, Right Upper Lung; LUL, Left Upper Lung; Mix type, BA with monolayered cell lesion; NA, not available.

BIOTECH, BEIJING, CO., LTD.). Fragments of BRAF (exon 15), KRAS (exons 2 and 3), and EGFR (exons 18, 19, 20, and 21) were detected by quantitative real-time polymerase chain reaction (Q-PCR). Q-PCR assays of target genes were performed on an Agilent Technologies Stratagene Mx3000P. Samples from 2 lesions were subjected to next-generation sequencing (NGS) using a panel of 61 and 733 cancer-related genes (Geneseeq-Prime, 3D Medicines, Inc., Shanghai, China), respectively.

Results

Clinical features

The clinicopathological characteristics of 17 cases of BA are summarized in Table 1. Among these 17 patients, five were from our center, and the remaining 12 were consultation patients. The median age was 57 years (range: 28-73 years), there were 7 men and 10 women, and 7 of the 17 patients had a history of smoking. Out of 17 lesions, 11 occurred in the right lung. On computed tomography (CT) scans, 4 lesions showed signs of ground-glass opacity (GGO) and 2 lesions showed ground-glass nodules (GGNs). Grossly, most BA lesions appeared as gray-white to taupe nodules with a mucoid appearance. The median gross tumor size was 1 cm (range, 0.2 to 5.3 cm). In addition, clinical follow-up was available for 17 patients with a median follow-up interval of 6 months (range: 0.5 to 28 months). None of the patients had local recurrence or distant metastases.

Pathological features

The 17 lesions were divided into proximal and distal types according to the proportion of mucous cells and ciliated cells in luminal cells. Out of 17 lesions, 9 were the proximal type, where 5 mainly had a flat structure, 1 mainly had a papillary structure, and 3 had both papillary and flat structures. The lesions with a predominant papillary structure had fibrovascular axes, and cells on the luminal surface of papillae were mainly composed of ciliated cells (Fig. 1A). In comparison, the luminal cells of the other proximal type were also predominantly composed of ciliated and mucous cells; however, they were mainly flat or duct-like in structure (Fig. 1B). Out of 9 proximal-type BA lesions, 7 had negative or weak staining for TTF-1 in luminal cells. Conversely, all proximal-type BA lesions had positive staining for TTF-1 in basal cells (Fig. 1A1,B1) as well as positive staining for P63 (Fig. 1A2,B2) and CK5/6 (Fig. 1A3,B3), thus suggesting that the lesions had basal cells. Four lesions were the distal type; they were characterized by a double-layer epithelium comprising basal cells and luminal cuboidal and club cells, and they lacked mucinous cells and ciliated cells (Fig. 1C). TTF-1 showed diffuse positivity in both luminal and basal cells in all 4 distal-type lesions (Fig. 1C1). P63 (Fig. 1C2) and CK5/6 (Fig. 1C3) were positively expressed in basal cells. In all lesions, the tumor cells showed no cytological atypia or increased mitotic activity, and the Ki67 index was <2%.

BA had other microscopic features (Fig. 2; Table 2). Overall, 88.2% (15/17) of the lesions had lymphoplasmacytic infiltration, which could appear in the periphery or the center of the lesion, indicating that it is inflammatory rather than septal. In contrast, only 29.4% (5/17) of lesions had ciliated micropapillae. In proximal-type BA lesions, the most common microscopic feature was lymphoplasmacytic infiltration (9/9; 100%). Correspondingly, the least common microscopic feature was discontinuous spread (2/9; 22.2%). Medium-sized arteries were present in only 1 out of 4 distal-type BA lesions. The microscopic features in distal-type BA were less common than those in proximal-type BA.

Among 17 cases, 4 cases did not have the complete classical morphology of BA, called putative variants of BA (Fig. 3). Two cases were judged to be mixed-type BA with monolayered lesions (Fig. 3A). Parts of the lesions had typical bronchiolar adenoma structures; however, they also showed areas where basal cells were missing, which consisted of a monolayer of mucous cells (Fig. 3A). These two regions were connected, and immunohistochemistry showed the following differences between them: TTF-1 (Fig. 3A1) was positive in double-layer structure areas, and it was weakly positive in monolayer mucinous cell structures. P63 (Fig. 3A2)

Table 2. Distribution of microscopic features in different types of BAs.

Microscopic features	Proximal-type (n=9)	Distal-type (n=4)	Mix type (n=2)	Monolayered type (n=1)	BA with invasive adenocarcinoma (n=1)	Totality (n=17)
Extracellular mucin production	(7/9) 77.8%	(2/4) 50.0%	(2/2) 100.0%	Yes	No	(12/17) 70.1%
Widening of the alveolar septa	(4/9) 44.4%	(2/4) 50.0%	(1/2) 50.0%	No	Yes	(8/17) 47.1%
Medium-sized artery	(6/9) 66.7%	(1/4) 25.0%	(1/2) 50.0%	Yes	Yes	(10/17) 58.8%
Discontinuous Spread	(2/9) 22.2%	(2/4) 50.0%	(2/2) 100.0%	No	No	(6/17) 35.3%
Ciliated micropapillas	(3/9) 33.3%	(1/4) 25.0%	(1/2) 50.0%	No	No	(5/17) 29.4%
lymphocyte infiltration	(9/9) 100%	(3/4) 75.0%	(1/2) 50.0%	Yes	Yes	(15/17) 88.2%
Basal cell hyperplasia	(4/9) 44.4%	(1/4) 25.0%	(1/2) 50.0%	No	No	(6/17) 35.3%

Mix type: BA with monolayered cell lesion.

revealed the absence of basal cells in the monolayer of the mucinous cell structure. Furthermore, HNF-4α (Fig. 3A3) was negative in the double-layer structure areas of bronchiolar adenomas and positive in the monolayer mucinous cell structure. One case in which there was neither stromal invasion nor the presence of basal cells was called a monolayered BA-like lesion (Fig. 3B). The lesion was composed entirely of monolayered columnar or cuboidal epithelial cells. Ciliated structures could be seen on the apical surface of the monolayer. These cells appeared mildly atypical. Immunohistochemistry showed that TTF-1 (Fig. 3B1) was positive in the monolayer mucinous cell structure. P63 (Fig. 3B2) revealed the absence of basal cells. Napsin A (Fig. 3B3) was negative in the monolayer mucinous cell structure. In addition, there was a case (Fig. 3C) in which BA showed significant cell atypia of luminal cells and a transformation from BA into invasive non-mucinous

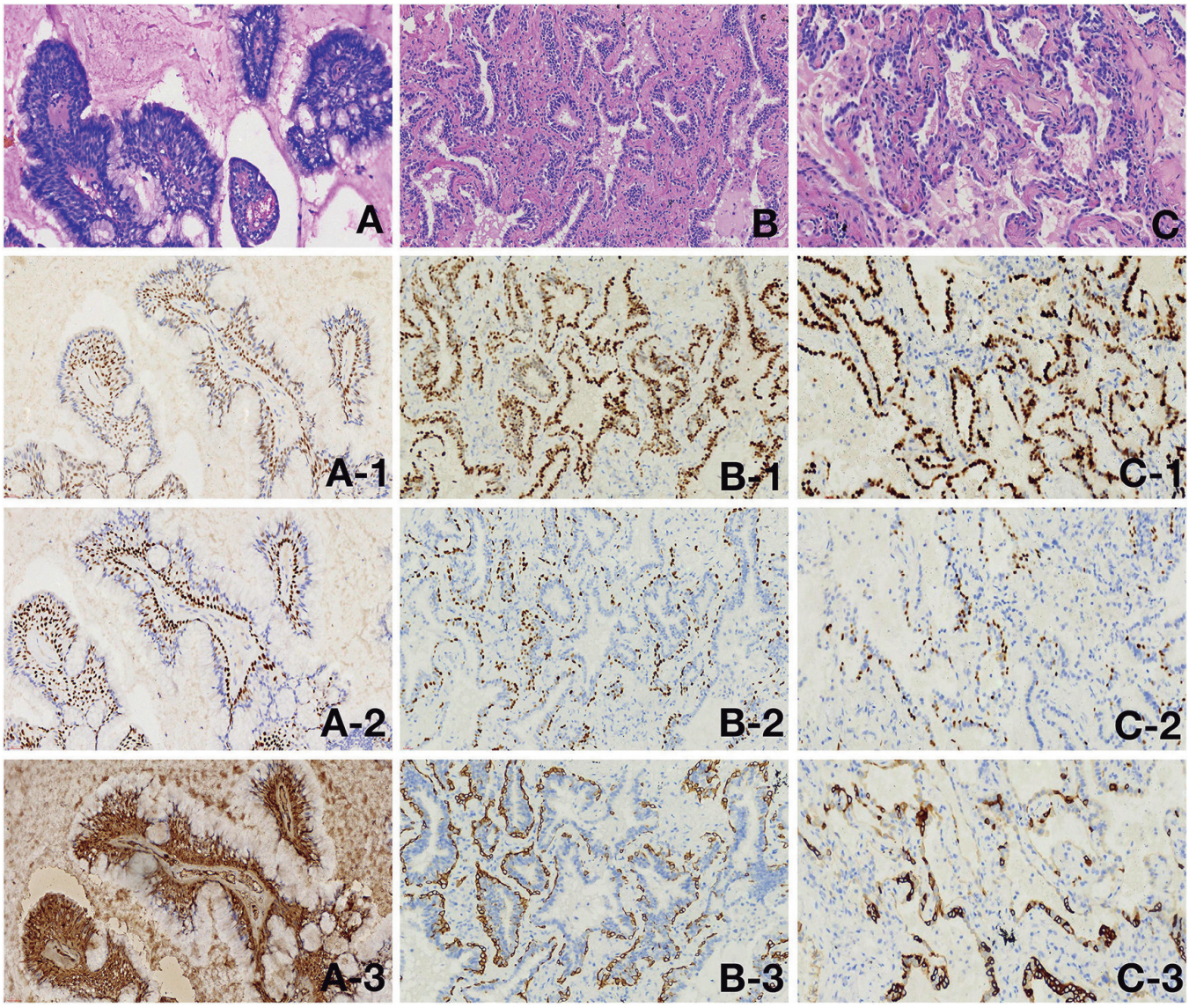

Fig. 1. Pathological features of bronchiolar adenomas. Proximal-type BA with papillary architecture. The papilla had a vascular fiber axis, and the lumen surface was columnar with cilia and mucous cells and contained a basal cell layer **(A)**; basal cells were positive for TTF-1, while luminal cells were negative or weakly positive for TTF-1 **(A-1)**; P63 **(A-2)** and CK5/6 **(A-3)** staining highlighted a continuous basal cell layer (Envision). Proximal-type BA with predominantly flat architecture. Tumor cells grew mainly flat along the alveolar wall and sometimes were accompanied by adenoid structures, and this tumor showed abundant ciliated cells **(B)**; TTF-1 **(B-1)** was expressed in basal cells and a few luminal nuclei but was weakly positive in mucinous cells; P63 **(B-2)** and CK5/6 **(B-3)** highlighted a continuous basal cell layer. Distal-type BA with entirely flat architecture lacked cilia and mucous cells, and most luminal cells had apocrine-like protrusions **(C);** TTF-1 **(C-1)** showed strong positivity in basal and luminal cells; P63 **(C-2)** and CK5/6 **(C-3)** showed a continuous basal cell layer (Envision). x 200.

adenocarcinoma (ADC). TTF-1 (Fig. 3C1) was positive in atypical luminal cells. P63 showed the presence of basal cells in some areas of this lesion (Fig. 3C2). P53 (Fig. 3C3) was positive in atypical luminal cells, and the results suggested that mutations in the *TP53* gene may exist in these cells.

Molecular Findings

In the present study, 3 out of 9 lesions had gene mutations. In one case, BA transformed into ADC, and the BA and adenocarcinoma areas were microdissected. DNA extracted from these two distinct areas was analyzed by NGS (a panel of 733 genes), and mutations in multiple genes of *TP53* p.R249S, *JAK2* p.V617F, *NF1* p.R416 and *RB1* p.S829 were found in both BA and adenocarcinoma. Positivity for the P53 antibody suggested that the *TP53* mutation was present at the protein level. To verify the role of other mutations, we detected the protein expression of NF, RB, and JAK2 by IHC (Fig. 4). In atypical luminal cells and adenocarcinoma cells, NF was negative (Fig. 4A), which suggested that mutation in *NF1* was not present at the protein level; in contrast, the loss of RB (Fig. 4B) and the overexpression of JAK2 (Fig. 4C) indicated that mutations in *RB1* and *JAK2* were present at the protein level. We further examined STAT3 phosphorylation in the JAK/STAT pathway, and p-STAT3 (Tyr705) (Fig. 4D) was positive in these cells, suggesting that the STAT pathway was activated. Moreover, one case of proximal-type BA with *BRAF* p.V600E mutation and one case of distal-type BA with *EGFR* ex19 p.L747_S752del mutation were identified. In our study, 1 case was mixed-type BA, and the bilayer structure and monolayer lesions were microdissected. These two distinct areas were analyzed by NGS (a panel of 61 genes), but no genetic mutations were identified in either part. No genetic mutations were found in monolayered BA-like

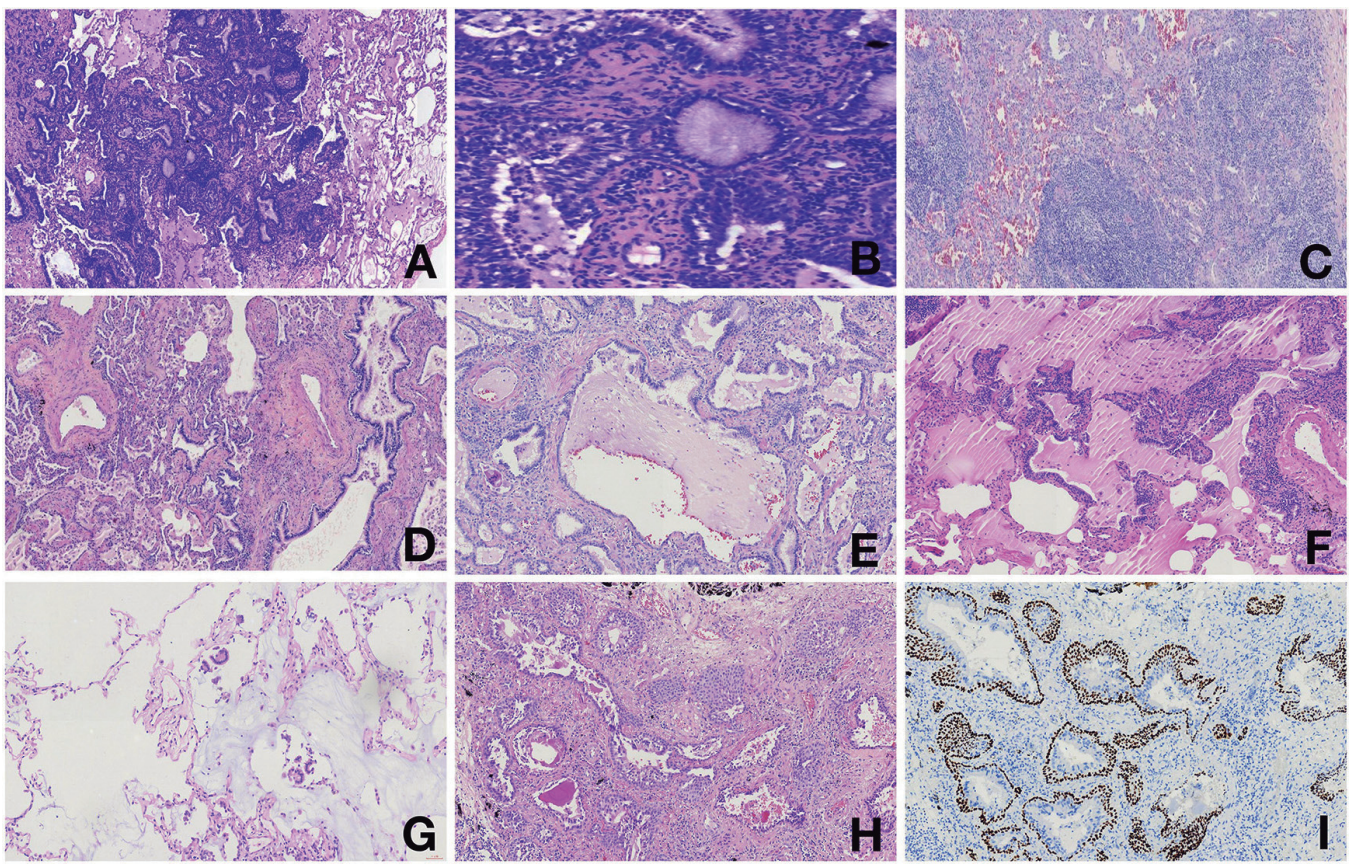

Fig. 2. Histological morphology of other changes in BA. The tumor periphery of proximal-type BA lesions was always accompanied by the formation of extracellular mucus lakes **(A)**. The stroma of BA can widen, forming an acinar-like appearance resembling adenocarcinoma; however, the widening stroma is attributed to edema and inflammatory lesions and lacks fibrosis **(B)**. BA was accompanied by infiltration of lymphocytes and the formation of lymphoid follicles **(C)**. There were often medium/small arteries passing through the tumor **(D)**. Similar structures to bronchioles could be seen in BA; their luminal cells were mainly composed of ciliated cells, and smooth muscle tissue could be seen around them **(E)**. The so-called discontinuous jumping growth was most likely to occur in the alveolar walls adjacent to the mucus lake or within the mucus lake **(F)**. Ciliated cellular micropapillary structures in BA lesions grew by sprouting and protruding into the alveolar space **(G)**. In proximal and distal lesions, basal cells could proliferate into multiple layers **(H)**. P40 highlighted a continuous basal cell layer **(I)**. A, x 100; B-I, x 200.

lesions by Q-PCR of fragments of *BRAF*, *KRAS* and *EGFR*.

We also reviewed seven previous studies (Kamata et al., 2016; Chang et al., 2018; Kataoka et al., 2018; Yang et al., 2020; Han et al., 2021; Sasaki et al., 2021; Shao et al., 2021) on BA. Together with our cases, molecular tests were performed on 80 lesions, and 62 of them had genetic mutations. The putative driver genetic mutations are summarized in Figure 5, including *EGFR* (n=25; 40.3%), *BRAF* (n=21; 33.8%), *KRAS* (n=10; 16.1%), and other genetic alterations (n=6; 9.7%). EGFR alterations included 14 cases with exon 19 deletions, among which eight driver mutations were p.E746_T751/S752>V and 3 were p.L747_S752del; other driver mutations were p.E746_S750del, p.E746_L747>IP, and p.G719S. Moreover, there were 10 cases with unusual exon 20 insertions, among which five driver mutations were p.N771_H773dup/insT and 2 were p.D773_N774insNPH; other driver mutations were p.N772_H773insYNP, p.A767_V769dup, and p.S768_D770dup. Out of 21 BRAF driver alterations, 20 were BRAF p.V600E, and in 1 case, the driver alteration was BRAF p.G606R. All KRAS mutations were missense mutations involving codon 10 (5 p.G12V; 4 p.G12D and 1 p.G12C). Finally, other genetic alterations consisted of two HRAS alterations, two *ERBB2* alterations and one *ERC1* alteration.

Discussion

BA is a benign tumor that has been recently included in the WHO (2021) classification of thoracic tumors (Nicholson et al., 2021). The concept of bronchiolar adenoma was first proposed by Chang et al. in 2018, after which BA was divided into proximal and distal types according to morphological and immunophenotypic characteristics (Chang et al., 2018). BA lacks specific clinical manifestations and has been associated with smoking, but in our study, less than half of the patients had a history of smoking. BA occurs more

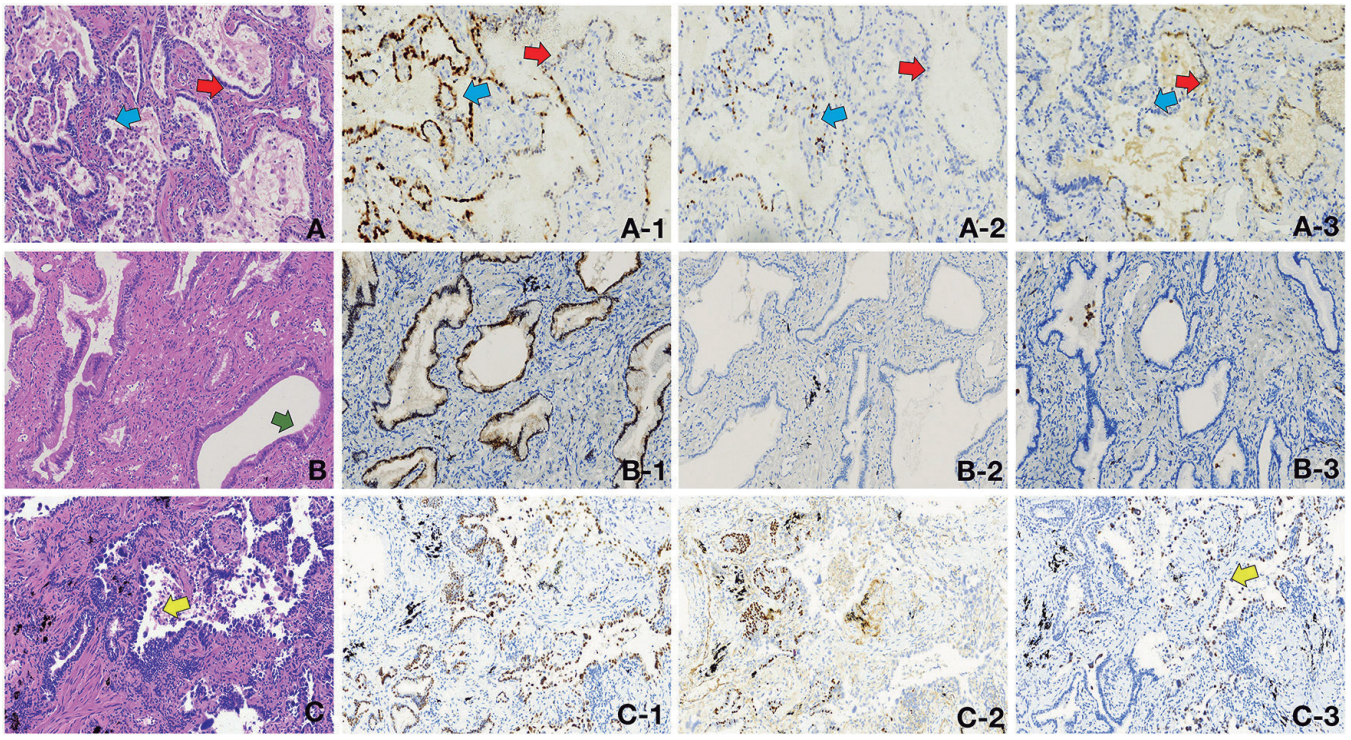

Fig. 3. Light microscope morphology and immunohistochemistry of the putative variants of BA. Mixed-type BA with monolayered lesions **(A)**. These lesions were rich in extracellular mucus and were mainly composed of glandular structures. Part of the region was composed of ciliated cells and mucous cells of the double-layer structure (red arrow); the other region was a single layer of mucous cell structure (blue arrow), with two areas connected. Immunohistochemical results showed that the expression of TTF-1 **(A-1)** in the monolayer structure decreased significantly or became negative; P63 **(A-2)** suggested the absence of basal cells in the monolayer structure; HNF-4α **(A-3)** was positive in the monolayer but negative in the double-layer structure. Monolayered BA-like lesion **(B)**. The lesion was composed entirely of monolayered columnar or cuboidal epithelial cells. The cells appear mildly atypical, and ciliated structures (green arrow) could be seen on the apical surface of the monolayer. TTF-1 **(B-1)** was positive in the lesion; P63 **(B-2)** suggested the absence of basal cells in the lesion; Napsin A **(B-3)** was negative in the lesion. The BA lesion transformed into invasive, non-mucinous adenocarcinoma **(C)**. Typical BA areas had a double-layer cell structure, which was the area of the adenocarcinoma where the cells were significantly atypical. Atypical luminal cells were found in the junctional zone between the BA and adenocarcinoma areas (yellow arrow). TTF-1 **(C-1)** was positive in atypical luminal cells and adenocarcinoma cells; P63 **(C-2)** suggested the presence of basal cells below the atypical luminal cells of the junctional region; P53 (**C-3)** was positive in atypical luminal cells and adenocarcinoma cells. x 200.

commonly in older women, and the youngest patient reported was 19 years old (Lau et al., 2016). In our study, the youngest patient was 28 years old. The imaging of BA often shows small ground-glass nodules (GGNs) in the lung parenchyma. In the present study, six lesions had ground glass-like features, including 4 with GGO and 2 with GGNs. Sun et al. differentiated BA and adenocarcinoma in situ (AIS) and MIA of the lung by CT texture analysis. In their study, the nodule type, tumor size, and pseudocavitation sign, which is a CT imaging feature of BA, showed significant differences between BA and AIS/MIA (Sun et al., 2021). Irregular shape, pseudocavitation, and ill-defined peripheral opacity were observed more frequently in BA (Cao et al., 2020). BA can potentially be misdiagnosed as carcinoma during intraoperative consultation. A multi-institutional retrospective review of frozen sections of BA/CMPT by Shirsat et al. showed that only 3 out of 18 cases were correctly diagnosed at the time of frozen section, all of which were proximal/classic type. At the same time, their study identified the features that were helpful in the diagnosis of BA in frozen sections, including a mixture of mild ciliated columnar cells, mucous cells, and the most important basal cell layer, as well as a lack of necrosis, marked atypia, and mitosis (Shirsat et al., 2021).

BA has no/mild atypia with a flat or papillary growth pattern under the microscope. Typical cases have a double-layer cell structure composed of a luminal surface and base, while atypical cases require a differential diagnosis. First, BA is most often confused with invasive mucinous adenocarcinoma (IMA), especially proximal BA lesions with flat structures and mucinous features. It is difficult to make distinctions in the diagnosis of frozen sections. Both BA and MIA can show discontinuous growth patterns, and both have mildly atypical cell structures. The most critical point in differentiation is the presence or absence of a continuous basal cell layer and ciliated cells (Shirsat et al., 2021). Second, BA can also be easily confused with acinar adenocarcinoma in frozen section diagnosis. Some cases of BA show interstitial widening, making alveolar walls close and resulting in adenoid structures. This phenomenon is a pitfall in the diagnosis of frozen

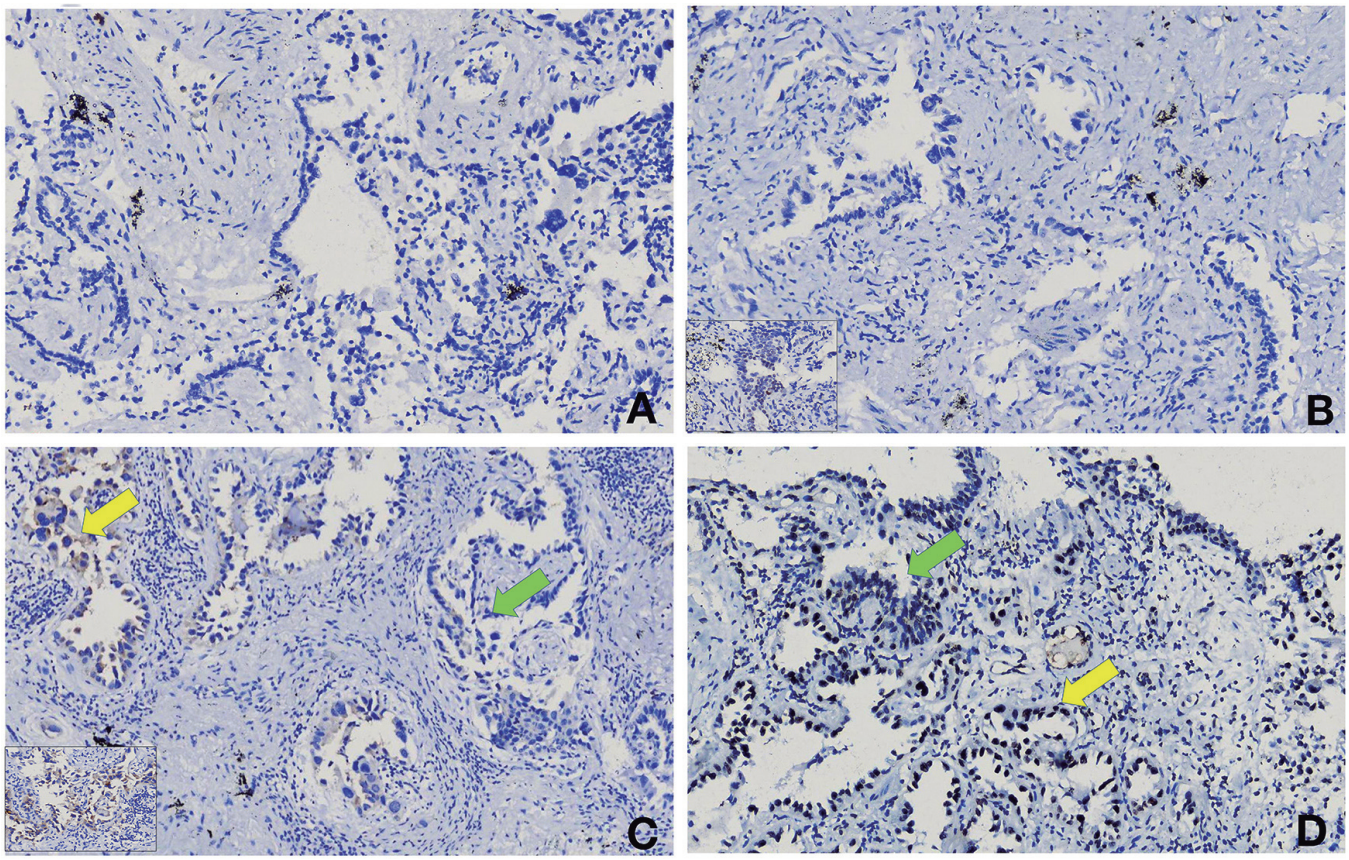

Fig. 4. Protein expression of mutations in multiple genes (*JAK2*, *NF1* and *RB1*) by IHC. One case may have transformed from BA to ADC: NF **(A)** was negative in atypical luminal cells and adenocarcinoma cells; RB **(B)** was lost in atypical luminal cells and adenocarcinoma cells, and the lower left image suggests that RB was not lost in normal cells; JAK2 **(C)** was weakly positive in atypical luminal cells (green arrow) and was positive in adenocarcinoma cells (yellow arrow, lower left image); p-STAT3 (Tyr705) **(D)** was positive in atypical luminal cells (green arrow) and adenocarcinoma cells (yellow arrow). x 200.

sections. However, many scholars have noted that inflammatory edema is the main cause of interstitial widening in BA, while the interstitial widening in adenocarcinoma is attributed to proliferating collagen fibers (Enhua, 2019; Gao et al., 2020). Third, both BA and micropapillary adenocarcinoma can present micropapillary structures that can stick to the alveolar walls or float in the alveolar space. Nevertheless, the micropapillary structure of BA is composed of ciliated cells and lacks cellular atypia, which was observed in 5 (29.4%) of our lesions. In contrast, micropapillary structures of adenocarcinoma often exhibit marked cellular atypia. The morphological features of BA are essential for differential diagnosis, which is very important in the diagnosis of frozen sections. The application of immunohistochemistry in diagnosing routine sections can assist in the diagnosis of BA. The most prominent feature is the continuous basal cell layer positive for P63/P40/CK5/6. In addition, the different expression of TTF-1 in the luminal cell layer and the basal cell layer is helpful for diagnosing and typing BA. Other microscopic features of BA are also important for diagnosis. For example, lymphoplasmacytic infiltration (15/17; 88.2%), extracellular mucin production (12/17; 70.1%), and medium-sized arteries (10/17; 58.8%) were found in more than half of the lesions in our study.

The high frequency of mutations in driver genes in BA indicates the clonal nature of these lesions. Moreover, the genetic profile of BA is heterogeneous. However, as there was a lack of large-scale induction and summary of putative driver mutation sites in BA, we summarized 62 lesions with gene mutations, including 59 reported in the previous literature from 71 lesions with molecular detection (Kamata et al., 2016; Chang et al., 2018; Kataoka et al., 2018; Yang et al., 2020; Han et al., 2021; Sasaki et al., 2021; Shao et al., 2021) and 3 lesions from the present study. EGFR gene mutation (25/62; 40.3%) was the most common genetic change in BA, with the most common being EGFR exon 19 (14/62; 22.6%) or 20 mutations (10/62; 16.1%); *EGFR* exon 21 p.L858R mutation was only reported in one case. Of the cases with EGFR mutations, the most common putative driver mutation was the *EGFR* exon 19 mutation (p.E746_T751/S752>V), which was also found in one of our cases (p.L747_S752del). In our study, alterations in BA were rare variants in lung adenocarcinoma, which were distinct from common sensitizing exon 19 deletions/exon 20 insertions of EGFR mutations. This finding was similar to that reported by Chang et al. (2018). The most common putative driver mutation site of BA was *BRAF* p.V600E (20/62; 32.3%). In addition, 10 cases had KRAS gene mutations. Most cases diagnosed with CMPT occurred before 2018, and the previous literature reported that *ALK* gene rearrangement appeared in CMPT (Jin et al., 2017; Taguchi et al., 2017). This is consistent with our summary of BA gene mutations. The most common mutations were *EGFR* and *BRAF* gene mutations; however, the driving mutation sites of *EGFR* were diverse, and they were different from the common mutation sites in lung adenocarcinoma.

Most of the previous literature supported that BA was a benign lesion with good patient survival, which is in line with our results. However, some studies have

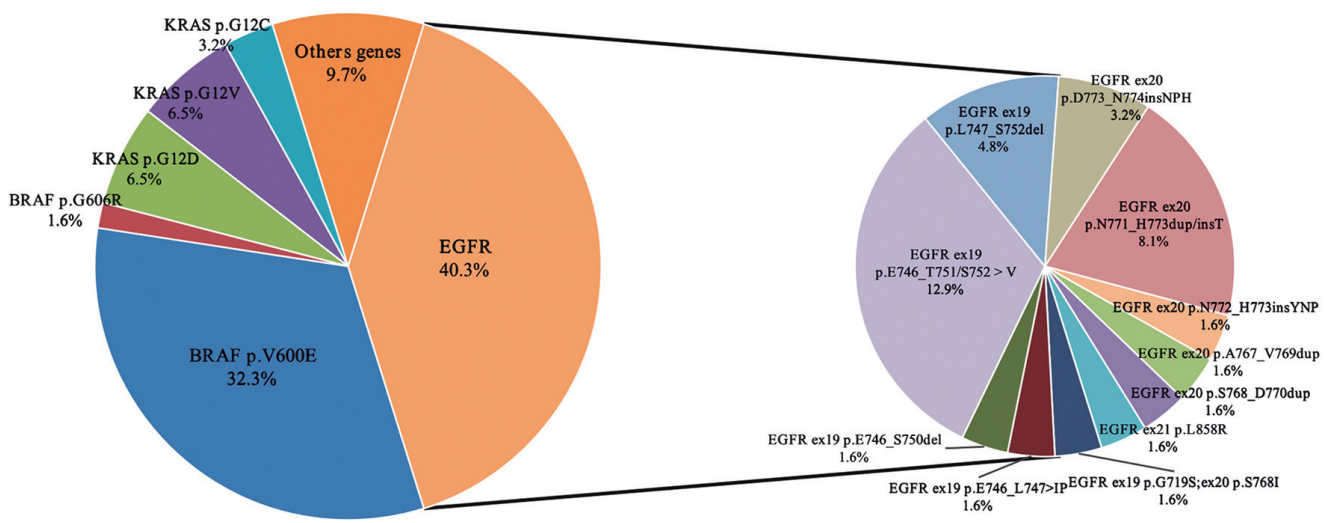

	Genetic mutations	n
Others genes	HRAS p.G12C /p.G13R	2
	ERBB2 p.G776delinsLC/p.Y772_A775dup	2
	ERC1 intron4-RET:intron11	1
	JAK2 p.v617F Exon14; NF1 p.R416 Exon11; RB1 p.S829 Exon23; TP53 p.R249S Exon7	1

Fig. 5. Distribution of putative driver mutations in 62 BA lesions in our study and the literature.

noted that CMPT/BA has malignant potential. Sun et al. reported a BA with a maximum diameter of 6.5 cm that did not require surgical management. After 3 months of follow-up, the patient was still alive, and the lesion did not shrink (Sun et al., 2020). The diameter of the largest lesion in our study was 5.3 cm. The patient underwent surgery and was followed up for 6 months. She was still alive without recurrence. In their study, Shao et al. proposed putative variants of BA (BA with monolayered cell lesions; monolayered BA-like lesions); these lesions likely reflected an ongoing process of malignant transformation from benign adenomas of bronchiolar epithelia. In addition, a high proportion of EGFR exon 20 insertions were found in BA with monolayered cells. The genetic characteristics of these BA variants were considerably different from those of classic BA (Shao et al., 2021). We quite agree with the above points. In our study, there were 2 lesions BA with monolayer cell structures. The monolayer cell structure lesion suggested that TTF-1 was focally weakly positive; yet, HNF-4α was positive. Such immunohistochemical results were similar to those of mucinous adenocarcinoma. However, no mutation was detected by NGS. We followed 2 patients for 2-4 months postoperatively, and both survived without recurrence. One of the lesions in our study was a monolayered BA-like lesion, which had mild cytological atypia and lacked the basal cell layer. Ciliated structures could be seen on the apical surface of the monolayer. TTF-1 was expressed on the monolayered BA-like lesion. This evidence suggests that the case has the potential to transition into a malignant tumor. Han et al. reported a case of BA with the same *KRAS* mutation as the adjacent IMA. In addition, the loss of continuity of the basal cell layer in the junctional zone between the BA and the IMA indicated malignant transformation from BA to IMA in this particular case (Han et al., 2021). To date, no convincing evidence has been found on whether BA can transform into ADC. We found a special case that may have transformed from BA to ADC. The luminal cells in the BA area were atypical, the basal cells transitioned from presence to absence, P53 was strongly positive in both the adenocarcinoma area and the atypical luminal cells, and the same genetic mutations (*TP53* p.R249S; *JAK2* p.V617F; *NF1* p.R416 and *RB1* p.S829) all suggest a malignant transformation from BA to ADC. Additionally, we found that mutations in *TP53*, *RB1* and *JAK2* were present at the protein level, suggesting that mutations in these genes may play a role in BA transformation into ADC. *TP53* was the gene most commonly mutated following *EGFR* in non-small cell lung cancer in the study by Chang et al. (2021). The effect of the *TP53* p.R249S mutant on proliferation in human hepatocellular carcinoma cells has been reported (Gouas et al., 2010). However, this mutation has not been reported in lung adenocarcinoma. Mutation in *RB1* p.S829 could cause nonsense-mediated mRNA degradation, resulting in loss of protein expression, thereby promoting the occurrence of malignancy (Yao et al., 2022). JAK2 variations have rarely been detected (10/1100; 0.9%) in lung adenocarcinoma patients, and JAK2 p.V617F mutation is the most common variation in the JAK2 gene (Xu et al., 2017). The JAK2 p.V617F mutation activates JAK2 kinase, which in turn activates the transcription signaling (JAK/STAT) pathway. The expression of p-STAT3 (Tyr705) indicates activation of the STAT3 pathway. STAT3 has been recognized as one of the key factors in tumor formation; in addition, overexpression of phosphorylated STAT3 has a significant correlation with poorer overall survival of lung cancer patients (Tong et al., 2017). We followed a patient for 28 months postoperatively who survived without recurrence. In summary, there have been case reports of a monolayer cell structure in some BA cases, and genetic evidence points to the possibility of BA to MIA transformation. Our study also indicates that BA can transform into ADC when the luminal cells of BA are atypical. In addition, the diagnostic terminology of BA was first proposed in 2018, and the follow-up time of all cases was <5 years, so additional data are needed for the long-term prognosis of BA. The putative variant of BA with a monolayer cell structure or pleomorphism of luminal cells is the top priority of follow-up.

Conclusion

BA is a rare type of disease. None of the reported cases had recurrence after surgery, and all had a good prognosis. Typical BA lesions have a double-layer cell structure and a continuous basal cell layer. Nonetheless, a putative variant of BA has a monolayer cell structure and lacks the basal cell layer. In the present study, the immunohistochemical expression of monolayer cell lesions was closer to that of MIA. A new discovery is that when the luminal cells of BA are atypical, transformation from BA to ADC may occur.

Conflict of interest. We declare that we have no financial or personal relationships with people or organizations that would inappropriately influence our work, and there is no professional or personal interest in any product, service and/or company that could be construed as influencing the position presented in, or the review of, our manuscript entitled "Clinicopathological features and genomic analysis of bronchiolar adenoma."

Funding. Supported by National Natural Science Foundation of China (81401882,82170082). Shanghai Municipal Science and Technology Commission 2021 Medical Innovation Research Project (21Y11908800). Clinical Research Project of Tongji Hospital of Tongji University (ITJ(QN) 1907). Research Project of Shanghai Putuo District Eastern integrated health care system (YLT2103).

References

Cao L., Wang Z., Gong T., Wang J., Liu J., Jin L. and Yuan Q. (2020). Discriminating between bronchiolar adenoma, adenocarcinoma in situ and minimally invasive adenocarcinoma of the lung with CT. Diagn. Interv. Imaging 101, 831-837.

Chang J.C., Montecalvo J., Borsu L., Lu S., Larsen B.T., Wallace W.D.,

Sae-Ow W., Mackinnon A.C., Kim H.R., Bowman A., Sauter J.L., Arcila M.E., Ladanyi M., Travis W.D. and Rekhtman N. (2018). Bronchiolar adenoma: Expansion of the concept of ciliated muconodular papillary tumors with proposal for revised terminology based on morphologic, immunophenotypic, and genomic analysis of 25 cases. Am. J. Surg. Pathol. 42, 1010-1026.

Chang Y.S., Tu S.J., Chen Y.C., Liu T.Y., Lee Y.T., Yen J.C., Fang H.Y. and Chang J.G. (2021). Mutation profile of non-small cell lung cancer revealed by next generation sequencing. Respir. Res. 22, 3.

Chen F., Ren F., Zhao H., Xu X. and Chen J. (2021). Mucinous adenocarcinoma caused by cancerization from a ciliated multinodular papilloma tumor: A case report. Thorac. Cancer 12, 1629-1633.

Enhua W. (2019). Bronchiolar adenoma: benign neoplasm easily confused with carcinoma. Chin. J. Pathol. 48, 8.

Gao H., Du X.L., Chen C.N., Song G.X., Gu Y.L. and Li H.X. (2020). bronchiolar adenoma: A clinicopathological analysis of 15 cases. Zhonghua Bing Li Xue Za Zhi. 49, 556-561.

Gouas D.A., Shi H., Hautefeuille A.H., Ortiz-Cuaran S.L., Legros P.C., Szymanska K.J., Galy O., Egevad L.A., Abedi-Ardekani B., Wiman K.G., Hantz O., Caron de Fromentel C., Chemin I.A. and Hainaut P.L. (2010). Effects of the TP53 p.R249S mutant on proliferation and clonogenic properties in human hepatocellular carcinoma cell lines: Interaction with hepatitis B virus X protein. Carcinogenesis 31, 1475-1482.

Han X., Hao J., Ding S., Wang E.H. and Wang L. (2021). Bronchiolar adenoma transforming to invasive mucinous adenocarcinoma: A case report. Onco Targets Ther. 14, 2241-2246.

Ishikawa Y. (2002). Ciliated muconodular papillary tumor of the peripheral lung: Benign or malignant? Pathol. Clin. Med. (Byouri-to-Rinsho) 20, 964-965.

Jin Y., Shen X., Shen L., Sun Y., Chen H. and Li Y. (2017). Ciliated muconodular papillary tumor of the lung harboring ALK gene rearrangement: Case report and review of the literature. Pathol. Int. 67, 171-175.

Kamata T., Sunami K., Yoshida A., Shiraishi K., Furuta K., Shimada Y., Katai H., Watanabe S., Asamura H., Kohno T. and Tsuta K. (2016). Frequent *BRAF* or *EGFR* mutations in ciliated muconodular papillary tumors of the lung. J. Thorac. Oncol. 11, 261-265.

Kao T.H. and Yeh Y.C. (2021). Ciliated muconodular papillary tumor/bronchiolar adenoma of the lung. Semin. Diagn. Pathol. 38, 62-71.

Kataoka T., Okudela K., Matsumura M., Mitsui H., Suzuki T., Koike C., Sawazumi T., Umeda S., Tateishi Y., Yamanaka S., Ishikawa Y., Arai H., Tajiri M. and Ohashi K. (2018). A molecular pathological study of four cases of ciliated muconodular papillary tumors of the lung. Pathol Int. 68, 353-358.

Lau K.W., Aubry M.C., Tan G.S., Lim C.H. and Takano A.M. (2016). Ciliated muconodular papillary tumor: A solitary peripheral lung nodule in a teenage girl. Hum. Pathol. 49, 22-26.

Miyai K., Takeo H., Nakayama T., Obara K., Aida S., Sato K. and Matsukuma S. (2018). Invasive form of ciliated muconodular papillary tumor of the lung: A case report and review of the literature. Pathol. Int. 68, 530-535.

Nicholson A.G., Tsao M.S., Beasley M.B., Borczuk A.C., Brambilla E., Cooper W.A., Dacic S., Jain D., Kerr K.M., Lantuejoul S., Noguchi M., Papotti M., Rekhtman N., Scagliotti G., van Schil P., Sholl L., Yatabe Y., Yoshida A. and Travis W.D. (2021). The 2021 WHO classification of lung tumors: Impact of advances since 2015. J. Thorac. Oncol. 17, 362-387.

Sasaki E., Masago K., Fujita S., Iwakoshi A., Kuroda H. and Hosoda W. (2021). AKT1 mutations in peripheral bronchiolar papilloma: Glandular papilloma and mixed squamous cell and glandular papilloma is distinct from bronchiolar adenoma. Am. J. Surg. Pathol. 45, 119-126.

Shao J., Yin J.C., Bao H., Zhao R., Han Y., Zhu L., Wu X., Shao Y. and Zhang J. (2021). Morphological, immunohistochemical, and genetic analyses of bronchiolar adenoma and its putative variants. J. Pathol. Clin. Res. 7, 287-300.

Shirsat H., Zhou F., Chang J.C., Rekhtman N., Saqi A., Argyropoulos K., Azour L., Simms A., Melamed J., Hung Y.P., Roden A.C., Mino-Kenudson M., Moreira A.L. and Narula N. (2021). Bronchiolar adenoma/pulmonary ciliated muconodular papillary tumor. Am. J. Clin. Pathol. 155, 832-844.

Sun Y., Liu M., Jiang Z. and Li B. (2020). Bronchiolar adenoma with diffuse pulmonary nodules: A extremely rare case report and review of literature. BMC Pulm. Med. 20, 192.

Sun J., Liu K., Tong H., Liu H., Li X., Luo Y., Li Y., Yao Y., Jin R., Fang J. and Chen X. (2021). CT texture analysis for differentiating bronchiolar adenoma, adenocarcinoma *in situ*, and minimally invasive adenocarcinoma of the lung. Front. Oncol. 11, 634564.

Taguchi R., Higuchi K., Sudo M., Misawa K., Miyamoto T., Mishima O., Kitano M., Azuhata K. and Ito N. (2017). A case of anaplastic lymphoma kinase (ALK)-positive ciliated muconodular papillary tumor (CMPT) of the lung. Pathol. Int. 67, 99-104.

Tong M., Wang J., Jiang N., Pan H. and Li D. (2017). Correlation between p-STAT3 overexpression and prognosis in lung cancer: A systematic review and meta-analysis. PLoS One 12, e0182282.

Xu Y., Jin J., Xu J., Shao Y.W. and Fan Y. (2017). JAK2 variations and functions in lung adenocarcinoma. Tumour Biol. 39, 1010428317711140.

Yang C., Wang X., Da J. and Ma K. (2020). Distal-type bronchiolar adenoma of the lung harboring an EGFR exon 21 p.L858R mutation: A case report. Thorac. Cancer 11, 3596-3598.

Yao Y., Gu X., Xu X., Ge S. and Jia R. (2022). Novel insights into RB1 mutation. Cancer Lett. 547, 215870.

Accepted March 17, 2023